*Article*

# Experimental Research on Collapsibility of Xi'an Loess Improved by Calcium Lignosulfonate

**Zhentao Bai [1], Dongbo Li [1]*, Dong Zhao [1], Wei Lu [1] and Jiaping Liu[2]**

[1] College of Science, Xi'an University of Architecture and Technology, Xi'an 710055, China; bzt@xauat.edu.cn; zdxauat@163.com; luwei@xauat.edu.cn

[2] State Key Laboratory of Green Building in Western China, Xi'an University of Architecture and Technology, Xi'an 710055, China; liujiaping@xauat.edu.cn

* Correspondence: ldb@xauat.edu.cn

**Abstract:** Collapsibility is an inherent characteristic of loess, which is often treated by adding industrial materials such as cement and lime in engineering, it seriously damages the reclamation performance of soil. Degradable calcium lignosulfonate (CLS) has a good prospect in balancing soil stabilization and environmental protection. Therefore, this paper evaluates the collapsibility and mechanical characteristics of CLS improved loess based on the collapsibility test, grey correlation analysis, and unconfined compressive strength test. The results show that when the content is 3%, the stabilization effect is most obvious, and the collapsibility coefficient can be reduced by more than 95%. The order of grey correlation degree of collapsibility on each index is moisture content, void ratio, dry density, and CLS content from large to small. The unconfined compressive strength increases rapidly in the first 14 days and then decreases with the content. When the content is too high, the strength of improved loess is lower than that of plain loess. Combined with SEM, microstructure parameters, and X-ray diffraction analysis, the carbonate minerals can play the role of filling pores and connecting soil particles, which reduces the grain size of mineral composition and the thickness of the electric double layer and makes the structure more compact. The research results have scientific significance and application value for the ecological modification research and engineering application of soil.

**Keywords:** loess; calcium lignosulfonate; collapsibility; unconfined compression strength ; strengthening mechanism

## 1. Introduction

Loess is widely distributed in the central and western regions of China, covering more than 6% of the area[1]. It is mainly composed of quartz, clay minerals, dissolved salts, etc. The unique skeleton particle connection method leads to poor properties such as multiple pores and high compression[2]. Under the erosion and infiltration of rainwater, the salts in the loess are easily dissolved, resulting in the rearrangement of soil particles and collapsibility, which often causes geological hazards such as landslides and foundation instability[3].

A great deal of research has been carried out on the problem of loess collapsibility. For instance, physical methods include strong tamping and replacement filling, adding plant fibers to enhance collapsibility, but commonly the durability is poor [4,5]. The mixing of cement and other industrial materials will make the soil highly alkaline and contain heavy metal ions, causing serious damage to the surrounding environment and soil reclamation[6]. In addition, in recent years, related scholars have used nanomaterials and polymer materials to improve the loess. Although it can somewhat improve loess's ability to collapse, its expensive price prevents industrialization and widespread use. [7]. Therefore, the research of economical and environmentally friendly new soil improvement materials has become an important issue to solve the problem of loess collapsibility.

 doi:10.20944/preprints202212.0335.v1

Industrial lignin mainly comes from paper mill waste liquor and biofuel by-products. China's paper industry can get about 0.5 billion tons of industrial lignin per year. As a derivative of lignin, calcium lignosulfonate (CLS) contains various active functional groups and has good cohesiveness, chelating and anti-corrosive properties[8]. However, more than 95% of industrial lignin is discharged into rivers in the form of wastewater or directly concentrated and incinerated every year. If industrial lignin is utilized, it can solve the waste pollution problem and achieve large-scale ecological modification[9].

The improvement of the mechanical properties and durability of untreated soils has been the main focus of research on CLS-improved soils. Zhang et al.[10] used CLS to cure silts, and the results of unconfined compressive strength (UCS) and California bearing ratio tests showed that CLS could effectively improve the particle gradation and mechanical properties of silts. Yang et al. [11] investigated the durability of CLS-improved soils by water immersion disintegration test and freeze-thaw cycle test and concluded that the water stability and freeze-thaw durability of CLS-improved soils were significantly improved compared with untreated soils. Ceylan et al. [12] used CLS to treat low-plasticity clay in Iowa. The results showed that CLS can effectively improve the engineering properties of the soil and has been successfully applied to the curing and dust treatment of low-grade traffic roadbeds and pavements.

At present, the research on the improvement of loess is still in its initial stage. Wang et al. [13] found that CLS can effectively improve the cyclic shear deformation and liquefaction resistance of loess by dynamic triaxial tests for the structural characteristics of loess. He et al. [14] found that the permeability of CLS was significantly reduced when it was mixed into loess, which could effectively improve the engineering properties of loess. Hou et al. [15] studied the modification of loess in the Lanzhou area and concluded that CLS can react with clay minerals in loess to produce quartzite and carbonate minerals, which makes the soil structure denser.

Although studies have been conducted to show that CLS can better improve the mechanical properties and engineering characteristics of loess, little research has been done on the characteristics of loess collapsibility under a low degree of compaction. As a result, CLS was chosen as the improved material in this study, and the change law of the collapsibility coefficient, the mechanical characteristics of the CLS improved loess, and the correlation between the major physical indices and collapsibility coefficient were all investigated. The results were also based on the scanning electron microscope test (SEM), microstructure parameters, and X-ray diffraction test (XRD) to elucidate the strengthening mechanism of CLS-improved loess. The results provide a reference for the engineering application in collapsibility loess areas.

## 2. Materials and Test Methods

### *2.1. Materials*

The soil samples were extracted from a highway project site in Xi'an, Shaanxi, China, at a depth of 3-4 m. The soil was crushed and air-dried, and then passed through a 2 mm sieve. The basic physical properties of the loess were determined according to ASTM D4318 standard[16], as shown in Table 1. Its optimum moisture content and maximum dry density were obtained by compaction tests as 18.0% and 1.69 g/cm$^3$, respectively.

Preprints (www.preprints.org) | NOT PEER-REVIEWED | Posted: 19 December 2022 doi:10.20944/preprints202212.0335.v1

**Table 1.** Basic physical indexes of tested loess.

| Property | Value |
|---|---|
| Water content /% | 2.87 |
| Density/(g·cm-3) | 1.17 |
| Liquid limit /% | 47.2 |
| Plastic limit /% | 35.5 |
| Plasticity index | 11.8 |
| Specific gravity | 2.70 |
| Clay (<0.002 mm) | 19.56 |
| Silt (0.002–0.074 mm) | 79.21 |
| Sand (0.074–2 mm) | 1.23 |
| Maximum dry density /(g·cm-3) | 1.69 |
| Optimum moisture content /% | 18.0 |

The CLS utilized in this investigation (Figure 1) was produced by Shanghai Maclean Biochemical Technology Co., Ltd. It was a solid brownish powder with a certain viscosity and fragrant odor that was readily soluble in water. Table 2 and Figure 2 show the main components and microscopic morphology of CLS respectively.

**Figure 1.** Calcium lignosulfonate (CLS) used in the test.

**Table 2.** Composition of CLS in the test.

| Molecular formula | Molecular weight | Lignin content /% | moisture /% | carbon content /% | sulfur content /% | pH |
|---|---|---|---|---|---|---|
| $C_{20}H_{24}CaO_{10}S_2$ | 528.61 | ≥96 | 5 | 40 | 5 | 7.00 |

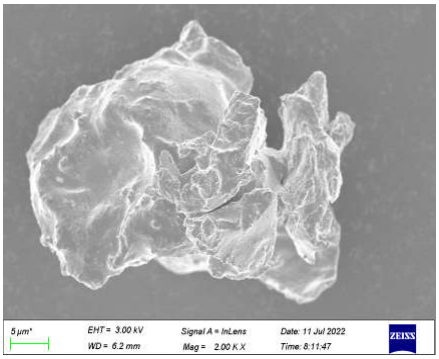


**Figure 2.** Microstructure of CLS.

*2.2. Sample Preparation*

The collected natural soil was air-dried and broken down by crushing with a rubber hammer. The particle size could be passed through a 2 mm sieve to remove any over-

Preprints (www.preprints.org) | NOT PEER-REVIEWED | Posted: 19 December 2022 doi:10.20944/preprints202212.0335.v1

sized particles in the experiment. Different amounts of CLS (0,1,3,5,7%) were mixed directly into the loess; the amount was the ratio of the modifier to the mass of dry soil. In order to ensure the uniform distribution of the modified additives, the mixtures were mixed manually for about 5 min after adding quantitative distilled water, and the configured soil samples were placed in vinyl bags and sealed for 24 h. The configured improved loess was then placed into the steel mold for the desired test and compacted by the static compaction method. The degree of compaction of the specimens prepared according to ASTM D698 was 0.85[17].

### *2.3. Testing Methods*

#### 2.3.1. Collapsibility Test

The collapsibility test was performed with a WG single-lever consolidation instrument produced by Nanjing Soil Instrument Factory. The test process was carried out in accordance with the provisions of the collapsibility test in GB 50025-2018[18]. The size of the cutting ring used for the specimens was Φ79.8mm× 20mm; the improved loess samples used for the tests were carried out with the optimum moisture content. The collapsibility characteristics of CLS improved loess were analyzed by the single and double-oedometer methods.

#### 2.3.2. UCS Test

The UCS test used a YYW-II electric calcareous soil unconfined pressure instrument. The test procedure was carried out in accordance with the provisions of ASTM D4219-02 for the testing of unconfined compressive strength[19]. The specimens were loaded at a rate of 3mm/min and the size was Φ50mm×50mm cylindrical specimens.

#### 2.3.3. SEM Test

SEM test was performed using a Hitachi HITACHI SU8010 scanning electron microscope for microstructure testing at a magnification of 1000x. The specimen was taken from the center of the 28d UCS test block, and the specimen size was a square with a side length of 10mm. The samples were the first vacuum dried and surface sprayed with gold, and then the undisturbed fresh surface was taken for observation.

#### 2.3.4. XRD Test

The XRD test was performed using a D8 ADVANCE X-ray diffractometer from Bruker, Germany, to scan the untreated loess and 3% CLS improved loess samples, the principle of which is shown in Figure 3. The samples were in the form of powder and had no obvious granularity; they had been ground and put through a 200 mesh filter. The basic parameters of the diffractometer were Cu target, power 3kW, wavelength $\lambda$=1.54056 Å. The scanning speed was 2°/min and the scanning range was between 5° and 90°.

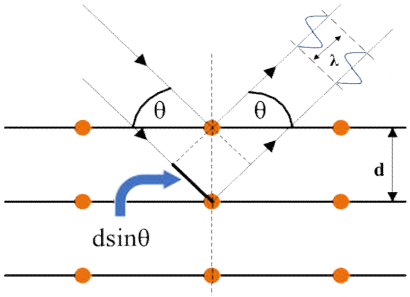


**Figure 3.** X-ray diffraction principle.

Preprints (www.preprints.org) | NOT PEER-REVIEWED | Posted: 19 December 2022 doi:10.20944/preprints202212.0335.v1

## 3. Results and Discussion

### *3.1. Collapsibility characteristics of improved loess*

The collapsibility coefficient is the ratio of the height difference between the soil before and after water immersion and the initial height of the soil under certain pressure, which is one of the important mechanical parameters to evaluate the collapsibility of loess. As expressed by the following equation:

$$\delta_s = \frac{h_p - h_{pb}}{h_0} = \frac{e_{pb} - e_p}{1 + e_0} \quad (1)$$

Where $h_p$ is added to a certain pressure, the height after sinking and stabilization; $h_{pb}$ is the specimen under the action of water immersion, the height after sinking and stabilization; $h_0$ is the initial height of the specimen; $e_{pb}$ is the pore ratio of the saturated specimen at a certain pressure; $e_p$ is the pore ratio of the original moisture content specimen at a certain pressure; $e_0$ is the initial pore ratio.

According to Equation (1), the collapsibility coefficient of improved loess under different pressures and admixtures is derived using the single and double-oedometer methods, respectively, as shown in Figure 4. As can be seen from the figure, the collapsibility coefficients measured by the two methods show the same trend of change. That is, at the pressure of 50 kPa, the CLS improved loess with different contents show strong collapsibility; with the increasing pressure, the collapsibility decreased significantly, and the collapsibility coefficient show a trend of rapid decrease and then stabilization. Under the pressure condition of 400kPa, the collapsibility coefficient of the improved loess with different CLS contents all drop to below 0.015, which behaves as non-collapsibility loess.

In addition, it can be seen from Figure 4 that the collapsibility coefficients obtained by the double-oedometer method are generally higher than those by the single-oedometer method. This is due to the different orders of immersion and loading, which present different results in the collapsibility process. The single-oedometer method is loaded and compressed first. The improved loess has tended to be dense and less porous. During the process of saturating with water, it is difficult for water to enter the soil particles and the collapsibility process is not sufficient[20]. The double-oedometer method is to load the improved loess sample when it is fully immersed in water, similar to the compression process of saturated soil. Due to the long immersion time, the salts and cementing substances in the CLS improved loess dissolve in water, and the collapsibility process proceeds more thoroughly, resulting in a significantly higher collapsibility coefficient [21].

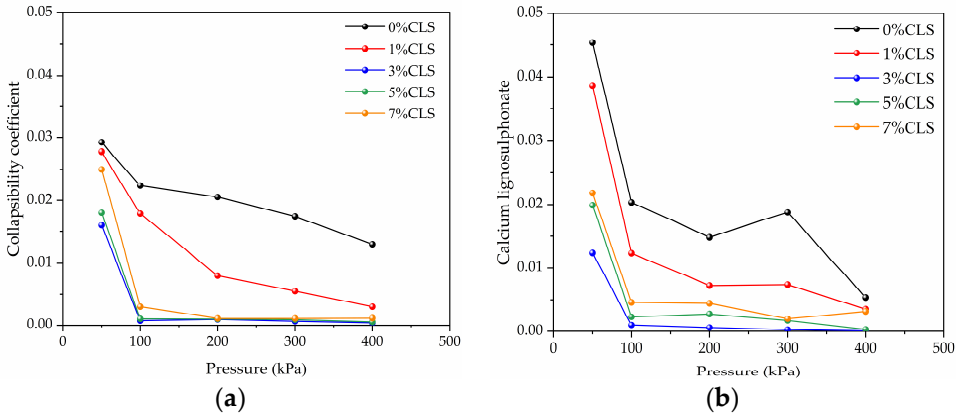


**Figure 4.** Collapsibility coefficient of improved loess with different content under various pressures. (**a**)single-oedometer method; (**b**) double-oedometer method.

As seen from the collapsibility test, the collapsibility of the improved loess upgraded significantly with the incorporation of CLS. In order to further objectively analyze the variation law between the collapsibility of improved loess with each basic physical index under standard pressure, the variation of collapsibility coefficient of improved loess with

Preprints (www.preprints.org) | NOT PEER-REVIEWED | Posted: 19 December 2022 doi:10.20944/preprints202212.0335.v1

moisture content (ω), dry density ($\rho_d$), pore ratio (e) and CLS content (θ) under 200 kPa pressure are plotted according to the test results, as shown in Figure 5.

As can be seen from the figure, the test results of single and double-oedometer methods remain consistent. The collapsibility coefficient is positively correlated with the pore ratio; negatively correlated with the dry density and moisture content.

There is no linear correlation between the content of CLS and the collapsibility coefficient, and the improvement effect is optimal when 3% CLS is added. In the single-oedometer method test, the collapsibility coefficient is reduced from 0.0206 in untreated loess to 0.0009 at 3% CLS content, a reduction of 95.63%. In the double-oedometer method test, the collapsibility coefficient decreased from 0.0148 in the untreated loess to 0.0006 in the 3% CLS doping, a decrease of 95.95%. With the further increase of CLS dosing, the collapsibility coefficient rebounds slightly, but it is still much lower than that of untreated loess.

It can be seen that the addition of CLS can effectively isolate the intrusion of water. This is because CLS contains a large number of lipophilic groups such as phenyl propane groups, which have a significant repulsive effect on water molecules[22]. In addition, CLS can fill the pores and connect soil particles to form a denser agglomerate, which can effectively reduce the permeability and dispersion of the improved loess.

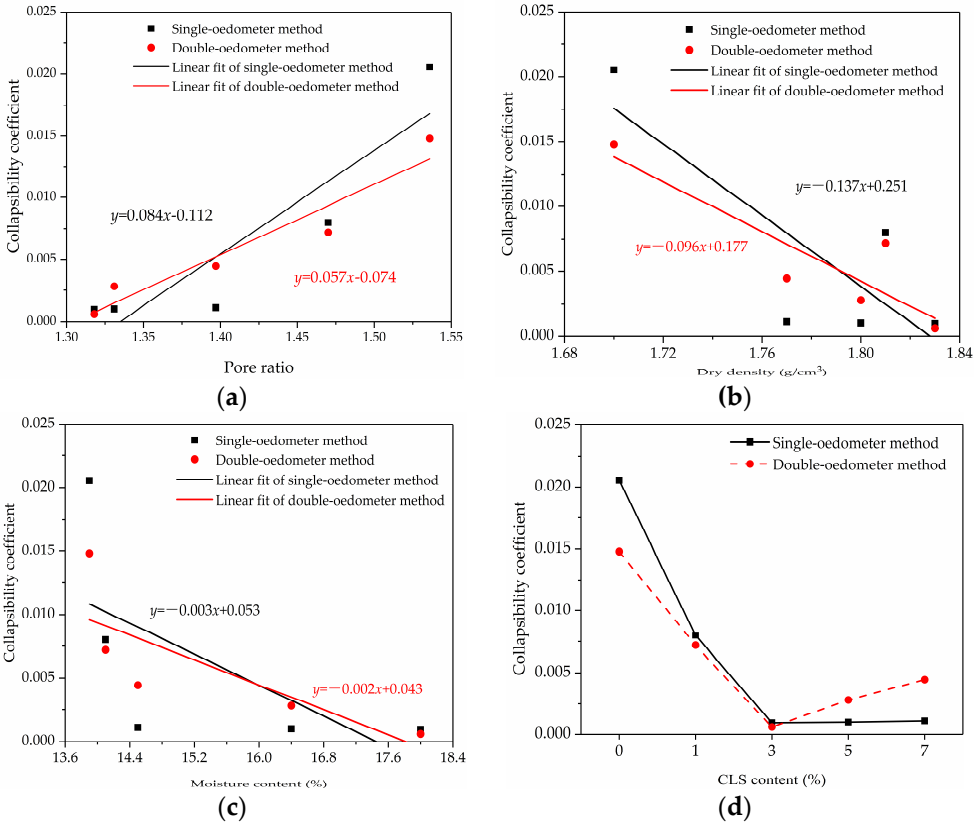


**Figure 5.** Relation between collapsibility coefficient and physical indexes at 200kPa.(**a**) pore ratio;(**b**) dry density;(**c**) moisture content;(d) CLS content.

### *3.2. Grey relational analysis of collapsibility*

From the results above, it is clear that the collapsibility of loess is influenced by a combination of factors[23]. However, inconsistencies in the units of measure and orders of magnitude of the parameters make it difficult to analyze the pattern of influence of the physical indicators on the collapsibility factor.

Gray system theory is an effective method to research information incomplete systems[24]. Gray correlation analysis is the core element of gray system theory, which is an analytical method used to characterize the degree of contribution of each influencing factor to the main behavior. Relational degree ($\gamma_i$) is the main parameter to characterize

Preprints (www.preprints.org) | NOT PEER-REVIEWED | Posted: 19 December 2022 doi:10.20944/preprints202212.0335.v1

the interrelationship between the factors of the system, the larger $\gamma_i$ indicates the stronger dependence of the parent sequence on a certain subsequence and the closer the relationship between them[25].

A gray correlation analysis is performed on the collapsibility loess after CLS improvement (Figure 6 shows the flow chart). Firstly, the parent sequence ($\delta_s$) and subsequences ($\varrho_d$, e, θ, ω) are determined; secondly, the range variation method is applied to eliminate the influence between the dimensions of each sequence, and the extremum ($\Delta_{max}$ and $\Delta_{min}$) are selected in the formed new sequence $\Delta_{ij}$; finally, the correlation coefficient matrix **L** and the relational degree $\gamma_i$ are calculated and then ranked for analysis.

Each factor in the correlation coefficient matrix **L** is calculated using the following equation:

$$l_{ij} = \frac{\rho\Delta_{\max} + \Delta_{\min}}{\rho\Delta_{\max} + \Delta_{ij}} \tag{2}$$

where $\rho$ is the resolution coefficient and $\rho \in (0,1)$ is usually taken as 0.5.

Due to the large and scattered data in the correlation coefficient, the analysis is not easy. Therefore, the correlation degree is defined as the average of the correlation coefficients and is calculated using the following equation:

$$\gamma_i = \frac{1}{n}\sum_{j=1}^{n} l_{ij} \tag{3}$$

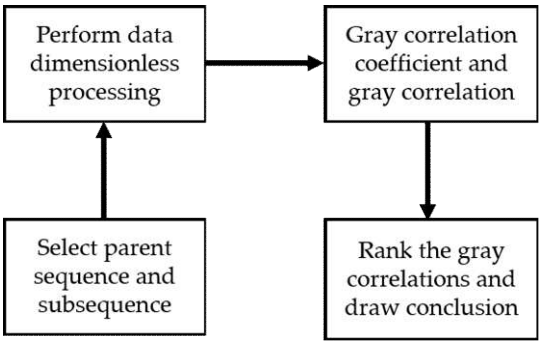


**Figure 6.** Flow chart of grey correlation analysis.

Table 3 shows the gray correlation values derive from the two collapsibility methods at a standard pressure of 200 kPa. As can be seen from the table, the correlation rankings derived from the single and double-oedometer methods are consistent, and the order of the sensitive factors of improved loess collapsibility coefficient is moisture content, pore ratio, dry density, and CLS content in that order.

The correlation order in this paper differs from the results of Wu et al.[26]. This is attributed to the difference between the untreated loess and the improved loess. The gray correlations of moisture content are 0.758 and 0.801, respectively, which rank first among the physical indicators. When the moisture content increases, there is not only strong combined water but also a certain amount of weak combined water between soil particles, which reduces the coulomb force and Van der Waals force between the particles and shows a decrease in cohesive forces from a macroscopic point of view. With the addition of CLS, the sensitivity of the soil to moisture content will gradually increase, making the moisture content the factor that most closely affects collapsibility[27]. Therefore, strict control of the water content of the CLS-improved soil is the key to preventing collapsibility.

The correlation between pore ratio and dry density on collapsibility coefficient is similar, which is also the main factor affecting the collapsibility of CLS-improved soil. The collapsibility coefficient is negatively correlated with dry density and positively correlated with the pore ratio[28]. It shows that when the dry density is larger, the pore ratio decreases, the soil structure is more compact, and the external water is difficult to enter to enhance its collapsibility.

Preprints (www.preprints.org) | NOT PEER-REVIEWED | Posted: 19 December 2022 doi:10.20944/preprints202212.0335.v1

Although the direct correlation between CLS content and collapsibility coefficient is the lowest, it is generally empirical that the correlation shows significance when the gray correlation is greater than 0.3[29]. With the incorporation of CLS, the maximum dry density of the improved loess increases, the optimum moisture content decreases, and the pore ratio decrease due to the filling of pores by CLS. The amount of CLS content indirectly affects the changes of each basic physical index and still has a significant improvement effect on the loess collapsibility.

**Table 3.** Grey correlation degree of physical indexes.

| Physical index | Single-oedometer method | Double-oedometer method |
|---|---|---|
| Moisture content $\omega$ | 0.758 | 0.801 |
| Pore ratio $e$ | 0.746 | 0.781 |
| Dry density $\rho_d$ | 0.73 | 0.76 |
| CLS content $\theta$ | 0.588 | 0.557 |

*3.3. Unconfined compressive strength of improved loess*

To further evaluate the curing effect of CLS-improved loess, UCS tests were conducted on improved loess with different CLS contents and curing ages.

As shown in Table 4 and Figure 7, at 1d, the strength difference between improved loess with different CLS contents is not significant and comparable to the strength of untreated loess (80.77 kPa). With the growth of the curing age, the UCS difference is gradually significant. The UCS of untreated loess at 1d, 14d, and 28d are 80.77kPa, 174.22kPa, and 235.99kPa, respectively, and the strength increases at 14d and 28d are 115.70% and 192.18%, respectively. The strength of the improved loess with 3% CLS content increases fastest, and its UCS at 1d, 14d, and 28d are 126.70kPa, 289.83kPa, and 354.77kPa, respectively, and the strength increases at 14d and 28d reach 128.75% and 180.01%, respectively. It can be seen that the untread loess and improved loess have the same growth trend with curing age, which means that the strength grows faster in the first 14 d, and grows slowly with stability in the last 14 d[30]. This is in agreement with the results of previous related studies, therefore, the curing age of the CLS-improved loess is guaranteed to be at least 14 d.

**Table 4.** UCS of improved loess under different CLS content and curing age.

| CLS content(%) | UCS(kPa) | | | |
|---|---|---|---|---|
| | 1d | 7d | 14d | 28d |
| 0 | 80.77 | 145.71 | 174.22 | 235.99 |
| 1 | 112.45 | 237.57 | 281.92 | 293.00 |
| 3 | 126.70 | 251.82 | 289.83 | 354.77 |
| 5 | 115.61 | 220.15 | 245.49 | 270.83 |
| 7 | 64.93 | 107.70 | 120.37 | 128.29 |

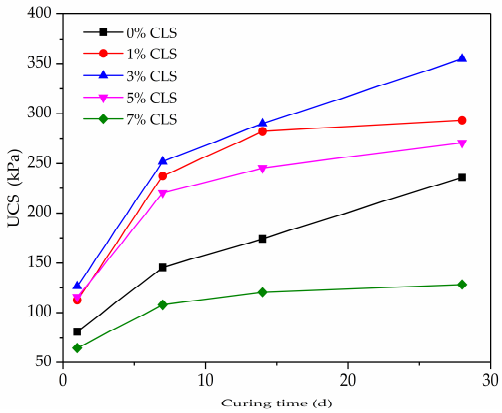


**Figure 7.** UCS of CLS improved loess.

 doi:10.20944/preprints202212.0335.v1

In addition, as shown in Figure 7, the UCS of the improved loess increases and then decreases with the content of CLS, and the maximum value is obtained when the content of CLS is 3% at the same curing age. When the content is too high, it will deteriorate the strength of the improved loess. For instance, when at 28d, the UCS of the improved loess with 7% CLS content is only 54.36% of that of the untreated loess. This is due to the fact that excess CLS preferentially forms agglomerates within the loess and that a large amount of CLS wraps around the soil particles, reducing the frictional resistance and skeletal strength between the soil particles[31].

## 4. Analysis of the strengthening mechanism of improved loess

### *4.1. SEM test analysis*

To better investigate the microstructure and strengthening mechanism of CLS-improved loess, SEM tests are conducted on the improved loess with different CLS content, as shown in Figure 8. As seen in Figure 8a, the untreated loess particles are angular and mainly show plate and granular shapes. The untreated loess is compacted, but still contains a large number of irregular aerial pores and intergranular pores. The structure type is skeleton-like, and the soil particles are associated with each other by direct point contact and direct surface contact[32]. When subjected to water erosion and pressure, the soluble salt dissolves, the overhead structure is damaged, and the soil particles in direct contact with each other stagger and slip are accompanied by local fragmentation, eventually leading to structural reorganization.

With the incorporation of CLS (Figure 8 b-d), the needle-like cementing materials began to develop, mainly concentrated in the particle connection and pores. A large number of overhead pores are filled with CLS, and the pore type is transformed into a closed type, which fills the pores and enhances the cohesion between the soil particles [33].

On the other hand, the fibrous CLS types of cementing materials are wrapped around the surface of soil particles, changing the soil particles from direct contact to indirect point contact and indirect surface contact linked by the cementing materials, and increasing the effective contact area. Preliminary studies have shown that the flocculation-like structure through indirect contact has better load-bearing performance and water stability than the skeleton-like structure through direct contact [34].

However, when the content of CLS is too large (Figure 8e), the CLS will combine itself to form agglomerates. Although the number of pores is reduced, the increase in pore size makes some of the soil particles separate from each other. The cohesion of the improved loess increases at this time, but the internal friction between the soil particles decreases sharply resulting in the reduced structural strength of the soil. The soil breaks more completely under external pressure, which leads to a change in both the collapsibility coefficient and the unconfined compressive strength.

Preprints (www.preprints.org) | NOT PEER-REVIEWED | Posted: 19 December 2022 doi:10.20944/preprints202212.0335.v1

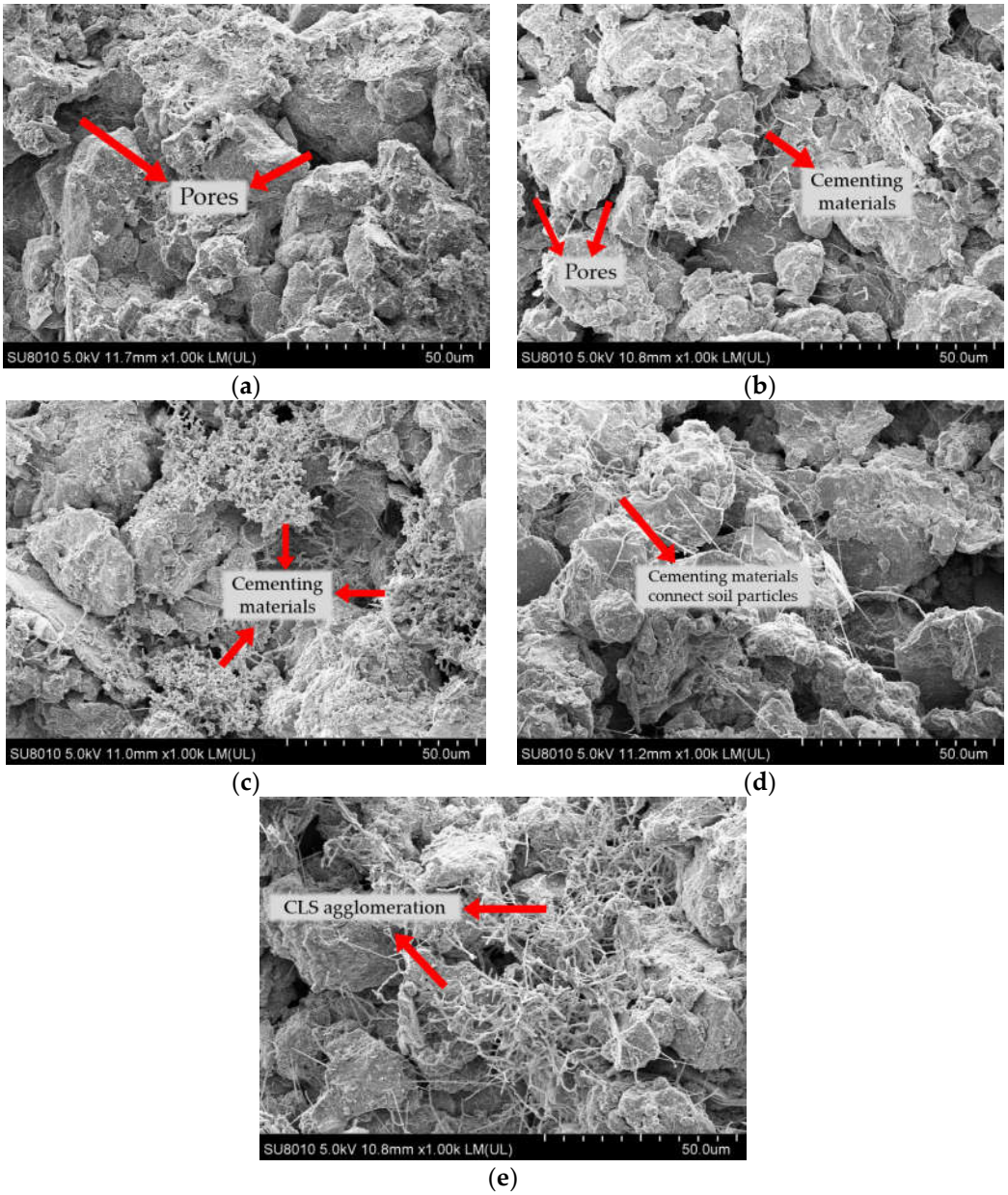


**Figure 8.** SEM results of improved loess with different CLS content. (**a**) untreated loess; (**b**) 1% CLS content; (**c**) 3% CLS content; (**d**) 5% CLS content; (**e**) 7% CLS content.

*4.2. Microstructure parameter analysis*

Although SEM images can show the differences between different CLS content improved loess from microscopic morphology and other aspects, it is difficult to quantitatively characterize indicators such as apparent pore ratio, probability entropy, fractal dimension value of porosity, and the relationship between microstructure and macroscopic properties.

For this purpose, this paper uses the particles (pores) and cracks analysis system (PCAS) to quantify and analyzes the SEM images. Firstly, the SEM images are automatically segmented by threshold and optimally adjusted; secondly, the soil particles and pores in the images are marked as black and white respectively by the binarization process (Figure9); finally, the binarized images are identified and statistically analyzed to quantify the microstructural parameters[35].

Preprints (www.preprints.org) | NOT PEER-REVIEWED | Posted: 19 December 2022 doi:10.20944/preprints202212.0335.v1

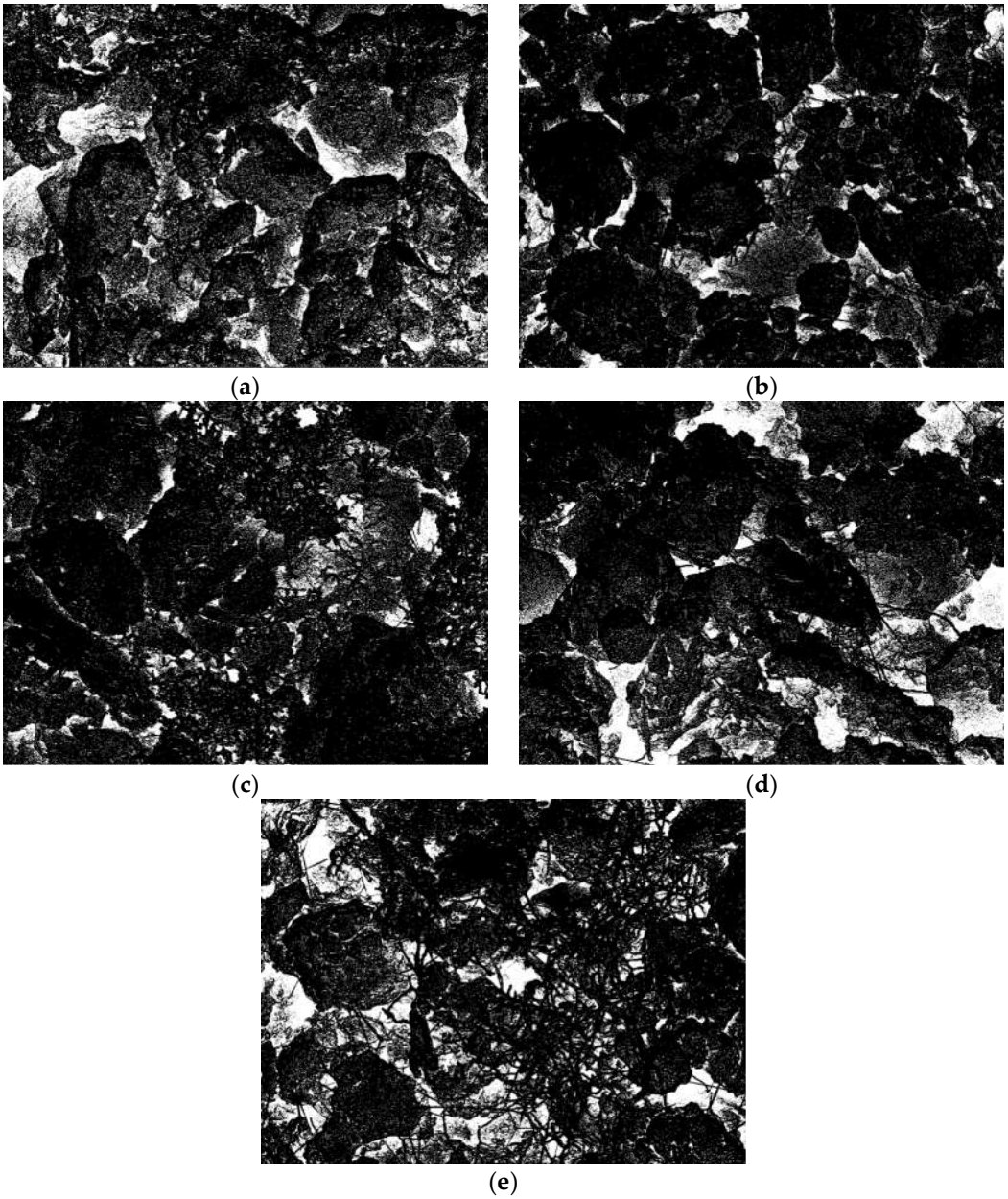


**Figure 9.** Binary image of improved loess with different CLS content. (**a**) untreated loess; (**b**) 1% CLS content; (**c**) 3% CLS content; (**d**) 5% CLS content; (**e**) 7% CLS content.

The apparent pore ratio is an important indicator of the degree of soil compactness and can be characterized computationally by using the ratio of pore area to soil particle area in the binarized image.

Figure 10 shows the apparent pore ratios of improved loess with different CLS content. As can be seen from the figure, with the increase in CLS content, the apparent pore ratio shows a trend of first decreasing and then increasing, and the lowest pore ratio is only 5.66% when the CLS content amount is 3%. As mentioned before, when the content is too high, CLS will produce its agglomeration phenomenon, increasing the distance between soil particles and deteriorating the compactness of the soil[36].

Preprints (www.preprints.org) | NOT PEER-REVIEWED | Posted: 19 December 2022 doi:10.20944/preprints202212.0335.v1

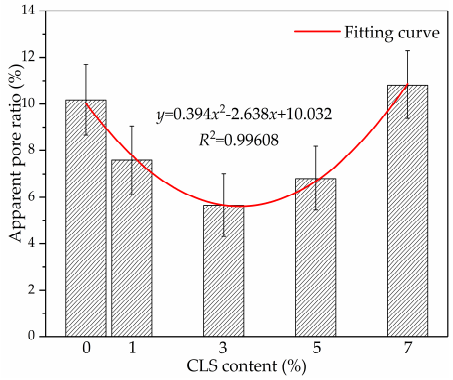


**Figure 10.** Apparent pore ratio of improved loess with different CLS content.

According to the results in Figure 10, the relationship between the content of CLS and the apparent pore ratio can be further fitted as:

$$y = 0.394x^2 - 2.638x + 10.032$$
$$R^2 = 0.99608 \quad (4)$$

From equation (4), it can be seen that the relationship between CLS content and apparent pore ratio is a quadratic polynomial. From equation (4), it can be theoretically calculated that the apparent pore ratio is the lowest when the content of CLS is 3.35%, indicating that the improved loess is in the densest state at this time, which is consistent with the macroscopic test results when the content of CLS is 3% in this paper.

Probability entropy is an index reflecting the degree of disorder of pore arrangement in soil, the smaller the probability entropy, the better the directionality and orderliness of pore arrangement[37]. The calculation formula is:

$$H_m = -\sum_{i=1}^{n} P_i \log_n P_i \quad (5)$$

Where $H_m$ is the probability entropy of the soil structure, taking values from 0 to 1; $P_i$ is the probability that the structural unit body is presented in a certain orientation zone.

Figure 11 shows the probability entropy of the improved loess with different CLS content. As can be seen from the figure, there is no obvious change in the probability entropy of improved loess with different CLS content. However, the probability entropy is relatively high for untreated loess, relatively low at 3% and 5% CLS content, and slightly rebounding at 7% CLS content. It shows that the pore arrangement in the soil tends to be regularized under the coupling effect of CLS. This is consistent with the SEM test results in this paper.

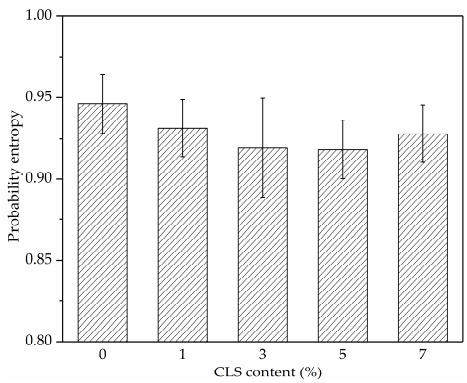


**Figure 11.** Probability entropy of improved loess with different CLS content.

Preprints (www.preprints.org) | NOT PEER-REVIEWED | Posted: 19 December 2022 doi:10.20944/preprints202212.0335.v1

The fractal dimension value of porosity is an index to characterize the distribution of pore size in the soil, the larger the fractional dimension value, the greater discrepancy of pore size in the soil. Its calculation formula is:

$$D_c = -\lim \frac{\ln N(r)}{\ln r} \tag{6}$$

Where $D_c$ is the fractal dimension value of porosity; $r$ is the pore diameter; $N(r)$ is the number of pores larger than this pore diameter.

Figure 12 shows the fractal dimension value of the porosity of the improved loess with different CLS content. As can be seen from the figure, the fractal dimension value of porosity shows a trend of decreasing and then increasing after the incorporation of CLS. The minimum value of porosity fractional dimension at 3% CLS content indicates that the particle structure in the improved loess is more closely distributed at this time, and the pore size and arrangement pattern tend to be unified. Compared to untreated loess, although it is compacted, the direct contact between soil particles leads to the existence of a large number of pores of different sizes[38]. Excessive CLS slightly reverted the porosity fractional dimension value due to weakening the filling effect of the improved loess, but the uniformity of the pore is still better than that of the untreated loess.

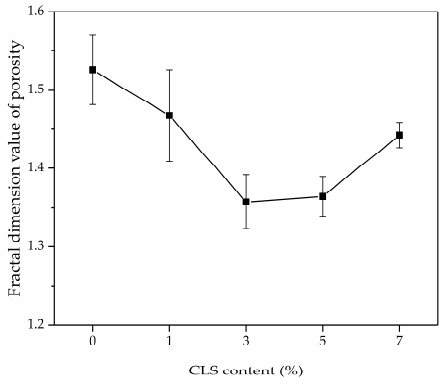


**Figure 12.** Fractal dimension value of porosity of improved loess with different CLS content.

*4.3. X-ray diffraction test analysis*

To investigate further the changes in mineral composition before and after the improvement of CLS, the X-ray diffraction method was used for the qualitative analysis of the phase of the untreated loess and the improved loess (CLS content of 3%).

Figure 13 shows the XRD test results of the untreated loess and the improved loess. As can be seen from the figure, there is no obvious change in the mineral composition before and after the action of the modifier, which is quartz, dolomite, calcite, and albite; and no obvious new mineral components are generated.

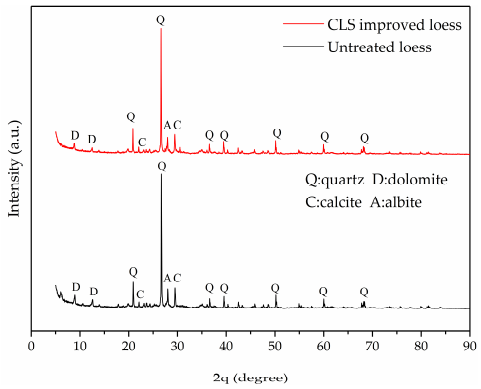


**Figure 13.** XRD analysis results.

Preprints (www.preprints.org) | NOT PEER-REVIEWED | Posted: 19 December 2022 doi:10.20944/preprints202212.0335.v1

It is noteworthy that although no new phases were generated after the improvement, the relative content of each mineral component was changed, as shown in Table 5. It can be seen that the content of dolomite (Ca Mg $(CO_3)_2$) and calcite (Ca $CO_3$) increased; the content of quartz ($SiO_2$) decreased and the content of albite (Na Al $Si_3O_8$) remained basically the same. Analyzing the reason, $Ca2^+$ ions in CLS react to form typical carbonate cementing materials such as (Ca Mg $(CO_3)_2$) and Ca $CO_3$, and the cementation strength of carbonate is higher than clay minerals, thus showing enhanced macroscopic properties.

**Table 5.** The mineral content of samples.

| Sample | Quartz (%) | Dolomite (%) | Calcite (%) | Albite (%) |
|---|---|---|---|---|
| Untreated loess | 43.3 | 24.6 | 11.8 | 20.4 |
| CLS improved loess | 38.1 | 28.7 | 12.6 | 20.6 |

To further investigate the strengthening mechanism of the CLS-improved loess, the grain size of each mineral component before and after CLS modification is calculated based on the XRD test results, and the results are shown in Table 6. It can be seen that the average grain size of each mineral composition is reduced after the incorporation of CLS, and the degree of reduction is more than 50%. The reduction in grain size is closely related to the structural changes in the soil and the degree of cementation between minerals[39]. It is inferred that under the effect of ion exchange and protonation (Figure 14), the positive charge of CLS neutralizes the negative charge on the soil surface, thus reducing the thickness of the double layer and making the mineral composition more aggregated and denser, which contributes to the improvement of soil strength and resistance to the effects of collapsibility[40].

**Table 6.** Calculation results of grain size of mineral composition.

| Mineral types | Before modification (nm) | After modification (nm) | Decrement (%) |
|---|---|---|---|
| Quartz | 371 | 185 | 50.13 |
| Dolomite | 301 | 123 | 59.14 |
| Calcite | 248 | 113 | 54.44 |
| Albite | 305 | 124 | 59.34 |

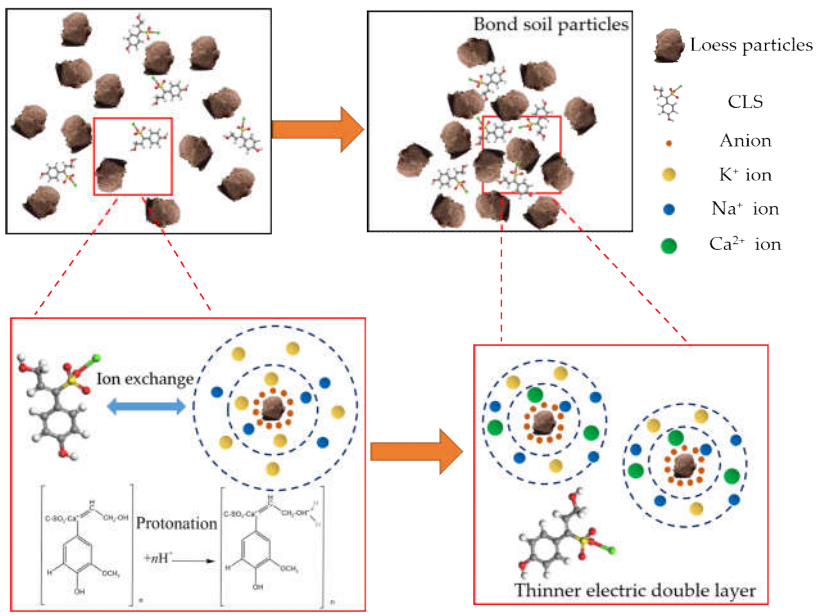


**Figure 14.** Schematic diagram of the mechanism of CLS improved loess.

 doi:10.20944/preprints202212.0335.v1

## 5. Conclusions

The present work investigated the laws of the influence of calcium lignosulfonate(CLS) on the collapsibility, gray correlation, unconfined compressive strength, and strengthening mechanism of loess in northwest China. The following conclusions can be highlighted:

(1) CLS contains lipophilic groups such as phenyl propane, which can still effectively improve the collapsibility of loess at a degree of compaction of 0.85. The optimal content of CLS selected in this paper was 3% when applied to improved loess, and the collapsibility coefficients were reduced by more than 95% in both single and double-oedometer methods.

(2) Loess collapsibility is determined by a combination of physical quantities such as substance composition and structural characteristics. According to the gray correlation analysis, the gray correlations of the factors affecting the collapsibility coefficient of improved loess were moisture content, pore ratio, dry density, and CLS content in descending order. Although the content of CLS was the smallest, the gray correlation was still more than 0.5 and showed a significant correlation, which can still effectively improve the collapsibility of loess.

(3) The unconfined compressive strength of the CLS-improved loess tended to increase and then decrease. The UCS was lower than the untreated loess when the CLS content was too high. The UCS continued to improve with the extension of the curing age, with rapid strength growth at the first 14 d.

(4) CLS made the improved loess dense and stable by filling pores, linking soil particles, and changing the way of connection between soil particles and the type of pores. By microstructural parameter analysis, the pore ratio and CLS content showed a quadratic polynomial relationship, and the probability entropy and fractal dimension value coincided with the macroscopic test results.

(5) The carbonate cement formed by the modification of CLS can effectively strengthen the soil structure; and under the effect of ion exchange and protonation, the thickness of the electric double layer was reduced and the grain size was reduced by more than 50%, making the mineral composition denser.

**Author Contributions:** Conceptualization, D.Z. and J.L.; methodology, Z.B.; validation, D.L., D.Z. and W.L.; formal analysis, Z.B.; investigation, Z.B.; resources, D.L. and W.L.; writing—original draft preparation, Z.B.; writing—review and editing, D.L. All authors have read and agreed to the published version of the manuscript.

**Funding:** This work was supported by the General program of National Natural Science Foundation of China (51878547); National Natural Science Foundation of China Youth Science Fund (52008332); China Postdoctoral Fund Regional Special Support Program(2021M693877).

**Institutional Review Board Statement:** Not applicable.

**Informed Consent Statement:** Not applicable.

**Data Availability Statement:** All data generated or analyzed during this study are included in this published article

**Conflicts of Interest:** The authors declare that they have no known competing financial interests or personal relationships that could have appeared to influence the work reported in this paper References.

## References


1. Luo, H.; Wu, F.; Chang, J.; Xu, J. Microstructural constraints on geotechnical properties of Malan Loess: A case study from Zhaojiaan landslide in Shaanxi province, China. *Engineering Geology* **2018**, *236*, 60-69, https://doi.org/10.1016/j.enggeo.2017.11.002.
2. Xu, L.; Coop, M.R.; Zhang, M.; Wang, G. The mechanics of a saturated silty loess and implications for landslides. *Engineering Geology* **2018**, *236*, 29-42, https://doi.org/10.1016/j.enggeo.2017.02.021.
3. Peng, J.; Wang, G.; Wang, Q.; Zhang, F. Shear wave velocity imaging of landslide debris deposited on an erodible bed and possible movement mechanism for a loess landslide in Jingyang, Xi'an, China. *Landslides* **2017**, *14*, 1503-1512, https://doi.org/10.1007/s10346-017-0827-6.
4. Feng, S.; Du, F.; Shi, Z.; Shui, W.; Tan, K. Field study on the reinforcement of collapsible loess using dynamic compaction. *Engineering Geology* **2015**, *185*, 105-115, https://doi.org/10.1016/j.enggeo.2014.12.006.
5. Peng, L.; Wang, D.; Qi, J. Study on anti-corrosion of PVA-treated wheat straw and its application in reinforcement of a silty soil. *Construction and Building Materials* **2021**, *291*, https://doi.org/10.1016/j.conbuildmat.2021.123305.
6. Wang, F.; Li, K.; Liu, Y. Optimal water-cement ratio of cement-stabilized soil. *Construction and Building Materials* **2022**, *320*, https://doi.org/10.1016/j.conbuildmat.2021.126211.
7. Tabarsa, A.; Latifi, N.; Meehan, C.L.; Manahiloh, K.N. Laboratory investigation and field evaluation of loess improvement using nanoclay – A sustainable material for construction. *Construction and Building Materials* **2018**, *158*, 454-463, https://doi.org/10.1016/j.conbuildmat.2017.09.096.
8. Ralph, J.; Lapierre, C.; Boerjan, W. Lignin structure and its engineering. *Curr Opin Biotechnol* **2019**, *56*, 240-249, https://doi.org/10.1016/j.copbio.2019.02.019.
9. Park, G.W.; Gong, G.; Joo, J.C.; Song, J.; Lee, J.; Lee, J.-P.; Kim, H.T.; Ryu, M.H.; Sirohi, R.; Zhuang, X.; et al. Recent progress and challenges in biological degradation and biotechnological valorization of lignin as an emerging source of bioenergy: A state-of-the-art review. *Renewable and Sustainable Energy Reviews* **2022**, *157*, https://doi.org/10.1016/j.rser.2021.112025.
10. Zhang, T.; Cai, G.; Liu, S. Application of Lignin-Stabilized Silty Soil in Highway Subgrade: A Macroscale Laboratory Study. *Journal of Materials in Civil Engineering* **2018**, *30*, https://doi.org/10.1061/(asce)mt.1943-5533.0002203.
11. Yang, B.; Zhang, Y.; Ceylan, H.; Kim, S.; Gopalakrishnan, K. Assessment of soils stabilized with lignin-based byproducts. *Transportation Geotechnics* **2018**, *17*, 122-132, https://doi.org/10.1016/j.trgeo.2018.10.005.
12. Ceylan, H.; Gopalakrishnan, K.; Kim, S. Soil Stabilization with Bioenergy Coproduct. *Transportation Research Record: Journal of the Transportation Research Board* **2010**, *2186*, 130-137, https://doi.org/10.3141/2186-14.
13. Wang, Q.; Zhong, X.; Ma, H.; Wang, S.; Liu, Z.; Guo, P. Microstructure and Reinforcement Mechanism of Lignin-Modified Loess. *Journal of Materials in Civil Engineering* **2020**, *32*, https://doi.org/10.1061/(asce)mt.1943-5533.0003422.
14. He, Z.; Henghui, F.; Junqiang, W.; Liu, G.; Wang, Z. Experimental study of engineering properties of loess reinforced by lignosulfonate. *Rock and Soil Mechanics* **2017**, *38*, 731-739, https://doi.org/10.16285/j.rsm.2017.03.015.
15. Hou, X.; Ma, W.; Li, G.; Mu, Y. Influence of lignosulfonate on mechanical properties of Lanzhou loess. *Rock and Soil Mechanics* **2017**, *38*, 18-26, https://doi.org/10.16285/j.rsm.2017.S2.003.
16. *ASTM D4318-10*; Standard test methods for liquid limit, plastic limit, and plasticity index of soils. ASTM: USA,2010.
17. *ASTM.D698*; Standard test methods for laboratory compaction characteristics of soil using standard effort. ASTM: USA,2012.
18. *GB50025-2018*; Building specification of collapsible loess region:. China Architecture and Building Press: Beijing,China,2018.
19. *ASTM D4219-02*; Test method for unconfined compressive strength index of chemical-grouted soils. ASTM: USA,2002.
20. Li, X.; Li, L.; Song, Y.; Hong, B.; Wang, L.; Sun, J. Characterization of the mechanisms underlying loess collapsibility for land-creation project in Shaanxi Province, China—a study from a micro perspective. *Engineering Geology* **2019**, *249*, 77-88, https://doi.org/10.1016/j.enggeo.2018.12.024.

21. Gao, C.; Du, G.; Liu, S.; Zhang, D.; Zhang, K.; Zeng, B. Field study on the treatment of collapsible loess using vibratory probe compaction method. *Engineering Geology* **2020**, *274*, https://doi.org/10.1016/j.enggeo.2020.105715.
22. Chen, Q.; Indraratna, B.; Carter, J.; Rujikiatkamjorn, C. A theoretical and experimental study on the behaviour of lignosulfonate-treated sandy silt. *Computers and Geotechnics* **2014**, *61*, 316-327, https://doi.org/10.1016/j.compgeo.2014.06.010.
23. Kuo, Y.; Yang, T.; Huang, G. The use of grey relational analysis in solving multiple attribute decision-making problems. *Computers & Industrial Engineering* **2008**, *55*, 80-93, https://doi.org/10.1016/j.cie.2007.12.002.
24. Deng, J. Control problems of grey systems. *Systems control letters* **1982**, *1*, 288-294, https://doi.org/10.1016/S0167-6911(82)80025-X.
25. Ren, S.; Wang, C.; Xiao, Y.; Deng, J.; Tian, Y.; Song, J.; Cheng, X.; Sun, G. Thermal properties of coal during low temperature oxidation using a grey correlation method. *Fuel* **2020**, *260*, https://doi.org/10.1016/j.fuel.2019.116287.
26. Wu, X.; Zhao, Y.; Xu, A.; Mi , W. Correlation of collapsibility of loess with physical indexes and evaluation methods. *Journal of Yangtze River Scientific Research Institute* **2018**, *35*, 75–80, https://doi.org/10.11988/ckyyb.20170160.
27. Cai, G.; Zhang, T.; Liu, S.; Li, J.; Jie, D. Stabilization Mechanism and Effect Evaluation of Stabilized Silt with Lignin Based on Laboratory Data. *Marine Georesources & Geotechnology* **2016**, *34*, 331-340, https://doi.org/10.1080/1064119X.2014.966217.
28. Zhang, T.; Liu, S.; Cai, G.; Puppala, A.J. Experimental investigation of thermal and mechanical properties of lignin treated silt. *Engineering Geology* **2015**, *196*, 1-11, https://doi.org/10.1016/j.enggeo.2015.07.003.
29. Wang, F.; Shi, H.; Huang, L.; Zhou, L. The technical system of biological measure on controlling of water and soil loss in hilly region of red earth. *Research of Soil and Water Conservation* **2005**, *12*, 248-251.
30. Kong, X.; Wang, G.; Liang, Y.; Zhang, Z.; Cui, S. The Engineering Properties and Microscopic Characteristics of High-Liquid-Limit Soil Improved with Lignin. *Coatings* **2022**, *12*, https://doi.org/10.3390/coatings12020268.
31. Zhang, T.; Yang, Y.L.; Liu, S.Y. Application of biomass by-product lignin stabilized soils as sustainable Geomaterials: A review. *Sci Total Environ* **2020**, *728*, 138830, https://doi.org/10.1016/j.scitotenv.2020.138830.
32. Ji, Y.; Ma, Q.; Li, X.; Tian, Y.; Cao, P. Study on Composite Improvement of Silt Sites by Lignin and Sodium Methylsilicate and Its Micro Mechanism. *Coatings* **2022**, *12*, https://doi.org/10.3390/coatings12111647.
33. Liu, Z.; Liu, F.; Ma, F.; Wang, M.; Bai, X.; Zheng, Y.; Yin, H.; Zhang, G. Collapsibility, composition, and microstructure of loess in China. *Canadian Geotechnical Journal* **2016**, *53*, 673-686, https://doi.org/10.1139/cgj-2015-0285.
34. Sun, Y.; Tang, L. Use of X-ray computed tomography to study structures and particle contacts of granite residual soil. *Journal of Central South University* **2019**, *26*, 938-954, https://doi.org/10.1007/s11771-019-4062-2.
35. Liu, C.; Tang, C.; Shi, B.; Suo, W. Automatic quantification of crack patterns by image processing. *Computers & Geosciences* **2013**, *57*, 77-80, https://doi.org/10.1016/j.cageo.2013.04.008.
36. Zhang, T.; Cai, G.; Liu, S. Assessment of mechanical properties in recycled lignin-stabilized silty soil as base fill material. *Journal of Cleaner Production* **2018**, *172*, 1788-1799, https://doi.org/10.1016/j.jclepro.2017.12.011.
37. Brus, D.J.; Bogaert, P.; Heuvelink, G.B.M. Bayesian Maximum Entropy prediction of soil categories using a traditional soil map as soft information. *European Journal of Soil Science* **2008**, *59*, 166-177, https://doi.org/10.1111/j.1365-2389.2007.00981.x.
38. Tang, C.; Lin, L.; Cheng, Q.; Zhu, C.; Wang, D.; Lin, Z.; Shi, B. Quantification and characterizing of soil microstructure features by image processing technique. *Computers and Geotechnics* **2020**, *128*, https://doi.org/10.1016/j.compgeo.2020.103817.
39. Alazigha, D.P.; Indraratna, B.; Vinod, J.S.; Heitor, A. Mechanisms of stabilization of expansive soil with lignosulfonate admixture. *Transportation Geotechnics* **2018**, *14*, 81-92, https://doi.org/10.1016/j.trgeo.2017.11.001.
40. Zhong, X.; Liang, Y.; Wang, Q.; Ma, J.; Liang, S.; Wang, Y.; Xu, X. Evaluation and Analysis of the Effect of Lignin Amelioration on Loess Collapsibility. *Journal of Renewable Materials* **2022**, *10*, 3405-3424, https://doi.org/10.32604/jrm.2022.021120.